Parameter Sensitivity Analysis of Small Rover Dynamics*

Bailey Hopkins[1] and Frankie Zhu[2]

***Abstract*— Future endeavors into space are using autonomous and controlled rovers to pave the way for human exploration. Understanding how rovers are affected by changes in the environment and their own design will help create a better breed of rovers. This paper conducts a sensitivity analysis for small-body rover dynamics using existing terramechanical models and numerical differentiation. Our results show that the rover's wheel width is the most impactful to a rover's motion in its environment. This analysis is for a specific set of reference parameters, and thus the methodology can be used to help guide the design of future spacecraft. The sensitivity analysis code is publicly available.**

I. INTRODUCTION

Designing a wheeled rover for a specific environment requires a thorough understanding of how the environment and the rover's attributes impact its mobility. As exploration of planetary surfaces advances, the development of autonomous and remote-controlled rovers becomes increasingly crucial and urgent; the NASA Volatiles INvestigating Polar Exploration Rover (VIPER) is slated to land on the Moon in 2024 [1], and the The Jet Propulsion Laboratories Cooperative Autonomous Distributed Robotic Exploration (CADRE) rovers [2] after VIPER. These mobile systems typically incorporate various components, such as wheels, suspension, and motor control methods, to navigate the challenging terrains encountered in these inhospitable environments. In this context, it is essential to comprehend the intricate interactions between these system elements and how environment site selection or modifications to a rover's design can influence this system's mobility. Therefore, the primary objective of this paper is to explore the relationships between the design attributes of wheeled rovers and environmental parameters to the rover's change in position, shedding light on the sensitivity of the rover's equations of motion to changes in these variables.

II. RELATED WORK

The Robotic and Space Exploration Lab (RoSE) at the University of Hawai'i at Mānoa has been investigating the mobility dynamics of small-body wheeled rovers. This paper leverages the derived equations of motion and estimated parameters from a physics-based dynamics model. Ishigami et al. [3] worked on a terramechanical model for the steering of rovers on loose soil; at the end of the paper, the authors noted that since soil parameters are not homogeneous, further study into an online determination of the parameters and sensitivity analysis of rover performance against variations in the soil parameters should be considered.

A. Equations of Motion

The following four forces are the primary forces acting on each wheel of the rover: normal force, lateral shear force, longitudinal shear force, and grouser force. These are contact forces that are derived from contact stresses acting on the surface of the wheel that are touching the local environment as shown in Fig. 1. Simulation environments, including Ishigami et al. [4] and Zhou et al. [5], use these forces to propagate the rover's dynamic state. While other forces do exist during wheeled locomotion, the authors have decided to focus on these four forces. However, the methodology outlined in this paper can be applied to other forces as needed. By summarizing these forces, it is possible to estimate the position of a wheeled rover $\vec{p}$ using Newton's Second Law of Motion in Eq. 1 where $\vec{F}$ is the sum of contact forces acting on all the wheels of a rover in the rover frame shown in Eq 2, where $\vec{F_n}$ is the normal force, $\vec{F_{\tau_x}}$ is the longitudinal shear force, $\vec{F_{\tau_y}}$ is the lateral shear force, and $\vec{F_g}$ is the grouser force.

$$\vec{p} = \int\int \frac{\sum \vec{F}}{m} dtdt \tag{1}$$

$$\sum \vec{F} = \vec{F_n} + \vec{F_{\tau_x}} + \vec{F_{\tau_y}} + \vec{F_g} \tag{2}$$

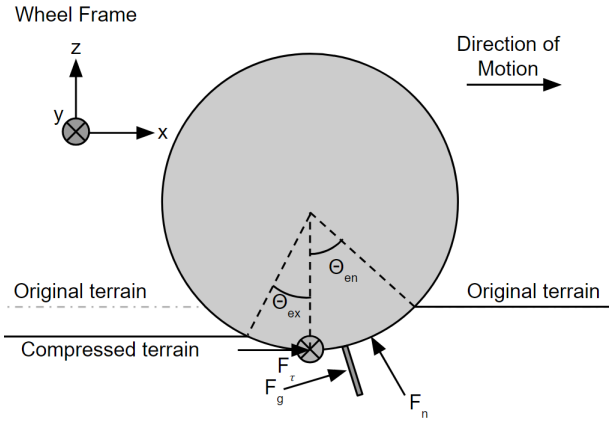

Fig. 1. Diagram showing a wheel's contact forces, F_n, F_τ, and F_g entry and exit angles, θ_{en} and θ_{ex}, and direction of motion within the wheel's reference frame. For skid steering rovers, rovers without actuating joints at wheels, the wheel frame is in the body frame of the rover.

*This work was supported by NASA Grant HI-80NSSC21M0334

[1]Bailey Hopkins is a Graduate Student of Mechanical Engineering at, the University of Hawai'i at Mānoa, USA bailey26@hawaii.edu

[2]Frances Zhu with the Hawai'i Institute of Geophysics and Planetology, University of Hawai'i at Mānoa, Honolulu HI 96822, USA zhuf@hawaii.edu

1) Normal Force: The normal force In our calculations is derived from the Reece and Wong equation for normal stress [6] [7]. Eq. 3 is the normal force acting on a wheel in the θ_{max} direction, where θ_{max} is given by Eq. 7.

$$\vec{F_n} = w_w w_r \left(\int_{\theta_{max}}^{\theta_{en}} \sigma(\theta) d\theta + \int_{\theta_{ex}}^{\theta_{max}} \sigma(\theta) d\theta \right) \quad (3)$$

The normal stress $\sigma(\theta)$, given by Eq. 4, is the Reece-Wong expression for normal stress with environmental parameters cohesion c, Bekker constant of cohesion K_c, density ρ, gravity g, Bekker constant of density K_p, rover parameters wheel width w_w and wheel radius w_r. Wheel entry angle θ_{en} and wheel exit angle θ_{ex} are parameters that can be measured in situ.

$$\sigma(\theta) = \begin{cases} (cK_c + \rho g w_w K_p)(\frac{w_r}{w_w})^n (\cos\theta - \cos\theta_{en})^n & \theta_{max} < \theta < \theta_{en} \\ (cK_c + \rho g w_w K_p)(\frac{w_r}{w_w})^n (\cos(\theta_{en} - \frac{\theta - \theta_{ex}}{\theta_{max} - \theta_{ex}}(\theta_{en} - \theta_{max})) - \cos\theta_{en})^n & \theta_{ex} < \theta < \theta_{max} \end{cases} \quad (4)$$

An expression for sinkage exponent n is given in Eq. 5, where n_0 and n_1 are sinkage parameters of soil and s is the slip ratio given by Eq. 6 where v is the linear velocity of a wheel and ω is the rotational velocity of the wheel.

$$n = n_0 + n_1 |s| \quad (5)$$

$$s = \begin{cases} 1 - \frac{v}{w_r \omega} & \text{if} \quad v < w_r \omega \\ \frac{w_r \omega}{v} - 1 & \text{if} \quad v > w_r \omega \end{cases} \quad (6)$$

Additionally, the term θ_{max} is used to describe the point along the wheel where the normal stress is at a maximum and is given by Eq. 7, where a_1 and a_2 are empirically determined model parameters [6] [7]. The form of the expression for θ_{max} is used to assist in addressing discontinuity issues that arise with the suggested form given by Wong and Reece [7].

$$\theta_{max} = (a_1 + a_2 s)\theta_{en} \quad (7)$$

2) Longitudinal and Lateral Shear Forces: Janosi and Hanamoto equations for shear stress [8] are given by Eq. 8 where α is either x for longitudinal shear force or y for lateral shear force.

$$\vec{F_{\tau_\alpha}} = w_w w_r \left(\int_{\theta_{ex}}^{\theta_{en}} \tau_\alpha d\theta \right) \quad (8)$$

For the longitudinal shear stress, the Janosi-Hanamoto equation for $\tau_x(\theta)$ is given by Eq. 9, where the maximum shear force τ_{max} is given by Eq. 10 and the shear displacement j_x is given by Eq. 11, where k_x is the shear deformation modulus.

$$\tau_x(\theta) = \tau_{max}(1 - e^{\frac{-j_x}{k_x}}) \quad (9)$$

$$\tau_{max} = c + \sigma(\theta)\tan\phi \quad (10)$$

$$j_x = \begin{cases} w_r(\theta_{en} - \theta - (1-s)(\sin\theta_{en} - \sin\theta)) & s \geq 0 \\ w_r(\theta_{en} - \theta - \frac{(\sin\theta_{en} - \sin\theta)}{(1+s)}) & s < 0 \end{cases} \quad (11)$$

Eq. 12 gives lateral direction expression where β is the lateral slip angle.

$$j_y = \begin{cases} w_r(1-s)(\theta_{en} - \theta)\tan\beta & s \geq 0 \\ \frac{w_r(\theta_{en} - \theta)\tan\beta}{(1+s)} & s < 0 \end{cases} \quad (12)$$

In practice, τ_y is only necessary for steering maneuvers and should have a negligible effect during straight-line driving.

3) Grouser Force: For grouser force, a modified version of the Wong expression is given by Eq. 13 [9], where the total force from the grousers is a summation of all individual grouser forces, $\vec{F_{g_i}}$, given by Eq. 14, and the total number of grousers in contact with the ground is χ, which is given by Eq. 15 rounded up to the nearest whole number.

$$\vec{F_g} = \sum_{i=1}^{\chi} \vec{F_{g_i}} \quad (13)$$

$$\begin{aligned} \vec{F_{g_i}} = w_w \{ & \frac{1}{2}\rho g h_g^2 (tan^2(\frac{\pi}{4} + \frac{\phi}{2})) cos\beta_g \\ & + q h_b (tan^2(\frac{\pi}{4} + \frac{\phi}{2})) \\ & + 2ch_g \sqrt{tan^2(\frac{\pi}{4} + \frac{\phi}{2})} \} \end{aligned} \quad (14)$$

$$\chi = \frac{(|\theta_{en}| + |\theta_{ex}|)(n_g)}{2\pi} \quad (15)$$

In the expression for grouser force, there is the height of the grousers h_g, the angle that the grouser makes with the soil β_g, and the internal friction angle ϕ. Additionally, soil surcharge q is related to the bulldozing of soil in front of the wheels. These equations represent the most common major forces that are used in modern simulation environments and expressions for comprehensive equations of motion describing terramechanics.

III. METHODOLOGY

A. Numerical Differentiation

To conduct sensitivity analysis, the partial derivative of the expression for the position in the x direction with respect to each of the 20 parameters, defined in Table I and Table II, is taken. The position function for a rover derived from

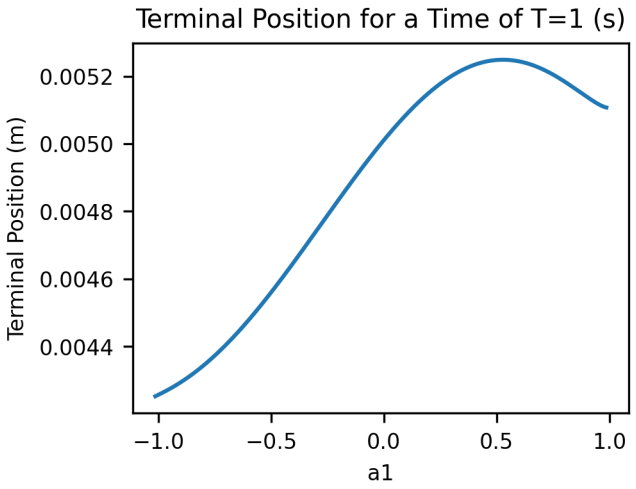

Fig. 2. Graph showing how the position of a rover propagated from Eq. 1 changes as the parameter a_1 changes for a propagation time of $T = 1$. The graph suggests that the curve is continuous, however, this is only for the window $-1 \leq a_1 \leq 1$ and needs to be verified.

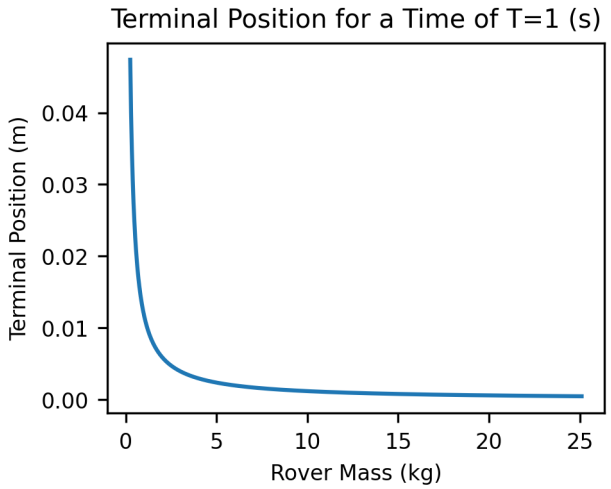

Fig. 3. Graph showing how the position of a rover propagated from Eq. 1 changes as the parameter m changes for a propagation time of $T = 1$. This graph shows that there is a discontinuity at $m = 0$ which is intuitively correct, however makes the function non-continuous and thus non-differentiable.

Newton's Second Law in this case does not lead itself to simple analytical derivatives. The plot in Fig. 2 was made by holing all parameters constant except for a_1 and determining where a rover would end up if it was allowed to drive forward for one second under these conditions. This was done for ranging values of a_1 to make the seemingly continuous curve. By making plots of the terminal position of a rover after one second while changing one parameter it can be shown how the expression reacts to changes in specific parameters. Fig. 2 shows the terminal as the parameter a_1 changes; this seems to have a continuous form and thus may have an analytical derivative. However Fig. 3 shows how the position changes with a change in mass, and there is a clear discontinuity at $m = 0$, thus no analytical derivative exists. For consistency, all derivatives were calculated numerically.

Numerical differentiation is used to calculate the partial derivatives; specifically, the symmetric difference quotient in Eq. 16 calculates the value of the partial derivatives at a reference or evaluation point.

$$\frac{\partial f}{\partial x} \approx \frac{f(x+h) - f(x-h)}{2h} \tag{16}$$

In this formula, a step size h needs to be chosen such that h is small enough to get close to the true derivative. Since these numerical derivatives are calculated in Python, there is a limit to how small the value of h can be. Because of this, a value of h needs to be determined such that h is small enough to approximate the derivative as closely to the true value while large enough to avoid numerical instability due to machine precision limits, given in Eq. 17 where ϵ is machine precision, and the second derivative is the slope of the secant line going through the points $f(x+h)$ and $f(x-h)$.

$$h = 2\sqrt{\epsilon|\frac{f(x)}{f''(x)}|} \tag{17}$$

In order to calculate h, the second derivative of the function is needed, which is a function of h, thus a loop is needed over a starting value of h and updates the value of the derivative and step size. To initiate, a selection of $h = 1E-06$ was selected and the loop ran for 1000 iterations, then the first 10 entries of the loop were discarded and the remaining 990 iterations were used to calculate the numerical mean of the partial derivative of the position function with respect to each variable. The standard deviation was also calculated to check convergence.

B. Reference Parameters

A baseline set of values is defined for the sensitivity analysis in Tables I andII. These reference values are selected from different sources, simulation environments, and small body rovers. For rover parameters shown in Table I, the RoSE Lab in-house rover Ka'a Holo Mahina (KHM rover) dimensions were used. The KHM rover is shown in Fig. 4 undergoing mobility testing. The design and form factor for the KHM rover were inspired by The Jet Propulsion Laboratories Cooperative Autonomous Distributed Robotic Exploration (CADRE) rovers [2]. Environmental parameters, shown in Table II, are from Zhou et. al [5]. The environmental parameters were selected from the study done by Zhou et. al. so that future work could have an experimental result from a lab outside of the RoSE lab to compare to. Note that the analysis done gives results for these specific initial conditions; if the analysis were to be done with a different rover or environment, the results may change.

Additionally to include the mass of the rover m in the list of parameters to consider, the partial derivatives need

to be taken from Eq. 1. This means that there needs to be a time component T that the expression for position needs to propagate to, in this study $T = 1sec$. This is an arbitrary selection, however, as with the starting selection of h, making T too small could lead to numerical instability. A smaller value of T would only change the magnitude of the partial derivatives and not affect their value or order when compared to the other parameters. If rover mass m is ignored then it is possible to take the partial derivatives of Eg. 2 and omit the dependency on T.

Fig. 4. Ka'a Holo Mahina undergoing mobility testing on O'ahu. VICON motion capture cameras are being used to track the position of KHM as it traverses a test area.

IV. RESULTS

Table III shows how a change in a rover's parameters contributes to a change in the rover's forward motion, while Table IV shows the effects of changing environmental parameters. The tables are organized such that the largest positive partial derivative is at the top and the largest negative partial derivative is at the bottom. The most influential parameters are the wheel width, then the height of the grousers, and lastly the entry angle of the wheel to the soil. All three of these values have positive values for their respective partial derivatives meaning that if one increases these values then one would expect to see the rover move further, or any errors in the values of these variables will yield a higher error in position estimates. The largest negative value (the largest contributor to hindering movement) is the rover's mass. It is important to note that these are the most influential parameters for a small body rover with the initial conditions outlined in Table I and Table II. For a different rover, either with different parameters or different geometry, the derivatives must be recalculated.

A. Limitations

The two largest influencers of the function were wheel width and the height of the grousers. Note this analysis

TABLE I

ROVER MODEL PARAMETERS WITH ASSOCIATED VARIABLE SYMBOL, REFERENCE VALUE, AND UNITS.

Parameter	Symbol	Value	Units
Wheel Width	w_w	0.00762	m
Height of Grousers	h_g	0.015	m
Wheel Radius	w_r	0.1	m
Number of Grousers	n_g	24	-
Rover Mass	m	2.28	kg

TABLE II

ENVIRONMENTAL MODEL PARAMETERS WITH ASSOCIATED VARIABLE SYMBOL, REFERENCE VALUE, AND UNITS.

Parameter	Symbol	Value	Units
Wheel Entry Angle	θ_{en}	0.0873	rad
Shear Deformation Modulus	k_x	0.029	m
Model Parameter	a_1	0.33	-
Internal Friction Angle	ϕ	0.5236	rad
Wheel Exit Angle	θ_{ex}	-0.0349	rad
Slip	s	0.1	-
Model Parameter	a_2	0.11	-
Gravitational Acceleration	g	9.81	m/s^2
Surcharge	q	0	-
Cohesion	c	0.2	kPa
Soil Mass Density	ρ	1650	kg/m^3
Bekker Coefficient of Density	K_p	212.2	-
Bekker Coefficient of Cohesion	K_c	677.5	-
Lateral Slip Angle	β	0.0175	rad
Shear Deformation Modulus	k_y	0.029	m
Nominal Sinkage Exponent	n_0	1.4	-
Slip-Sinkage Exponent	n_1	0.32	-

TABLE III

THE VALUES FOR THE PARTIAL DERIVATIVE OF THE POSITION EXPRESSION WITH RESPECT TO EACH ROVER PARAMETER.

Derivative	Value	Standard Deviation
$\partial p/\partial w_w$	$1.08E-01$	$4.05E-11$
$\partial p/\partial h_g$	$1.02E-01$	$6.09E-16$
$\partial p/\partial w_r$	$1.85E-03$	$2.80E-12$
$\partial p/\partial n_g$	0.00	0.00
$\partial p/\partial m$	$-3.82E-04$	$2.15E-17$

TABLE IV

THE VALUES FOR THE PARTIAL DERIVATIVE OF THE POSITION EXPRESSION WITH RESPECT TO EACH ENVIRONMENTAL PARAMETER.

Derivative	Value	Standard Deviation
$\partial p/\partial \theta_{en}$	$1.80E-02$	$5.33E-16$
$\partial p/\partial k_x$	$2.71E-03$	$6.87E-12$
$\partial p/\partial a_1$	$2.61E-03$	$5.61E-12$
$\partial p/\partial \phi$	$1.58E-03$	$1.15E-11$
$\partial p/\partial \theta_{ex}$	$3.64E-04$	$4.71E-12$
$\partial p/\partial s$	$2.62E-04$	$6.76E-17$
$\partial p/\partial a_2$	$2.61E-04$	$6.31E-17$
$\partial p/\partial g$	$8.86E-05$	$6.38E-13$
$\partial p/\partial q$	$6.27E-06$	$4.13E-18$
$\partial p/\partial c$	$1.58E-06$	$2.58E-19$
$\partial p/\partial \rho$	$5.27E-07$	$2.99E-14$
$\partial p/\partial K_p$	$5.12E-07$	$2.94E-14$
$\partial p/\partial K_c$	$8.30E-10$	$6.79E-21$
$\partial p/\partial \beta$	0.00	0.00
$\partial p/\partial k_y$	0.00	0.00
$\partial p/\partial n_1$	$-3.79E-05$	$8.24E-18$
$\partial p/\partial n_0$	$-3.79E-04$	$1.63E-17$

assumes all other parameters are held constant as that single parameter changes. This means that if the wheel width were to increase, the mass of the rover would not (in this analysis). While that may be a design consideration, it is important to remember that for a complex system when one variable changes, there may be an impact on other variables. Some notable examples are increasing the width of the wheels, and subsequently increasing the mass of the wheel and thus the mass of the rover. An increase in the mass of the rover will cause the rover to sink into the soil more and increase the entry angle of the wheel. This coupling caused by increasing one parameter dependency would be specific to the rover a researcher is working on and has not yet been fully explored by the authors but is a subject of future research.

There are two calculated results that are worth expanding on because they are unexpected. These results involve the number of grousers and the slip of the wheel. However, these parameters results seem to be a more direct result of the model used, and further exploration into these parameters is needed to identify potential flaws in adapting the model from large rovers to small-body rovers.

1) Number of Grousers: The partial derivative of position with respect to parameter n_g, the number of grousers, has a numerical value of 0. This means that any change to the number of grousers will have no effect on the position of a rover. This is misleading. In this analysis the entry and exit angles were 0.0873 radians and -0.0349 radians from normal respectively, meaning that only 0.1222 radians of the wheel were in contact with the soil. With 24 grousers on the wheel, there are 0.2618 radians between each grouser, and thus no two grousers are guaranteed to be fully in contact with the soil unless the number of grousers were to at least double. However multiple grousers may be partially in contact with the ground at any given time. This highlights a limitation of this model: discounting the number of grousers in partial contact with the ground at a given time. Fig. 5 shows how an increase in both the number of grousers and wheel entry angle creates a discontinuous relationship with the grouser force.

2) Slip: The partial derivative of the forward position with respect to slip has a positive value, which is counterintuitive to the definition of slip. This is due to the initial conditions that were selected. If one takes a look at how the individual forces are affected by slip, then one can see that the normal force decreases with an increase in slip. In contrast, the shear force in the x direction increases with an increase in slip. Subsequently, for the first small segment of slip (between 0 and 0.175), there is a slightly positive relation between slip and forward motion as the effect of the normal force is minimized. This effect is only apparent when inspected closely and is overshadowed by other dominant changes, such as when the slip is greater than 0.175, the downward trend appears. A visualization of how each force is affected by slip can be seen in Fig. 6 and how the motion of the rover is affected by slip is shown in Fig. 7. This phenomenon is a byproduct of the selected mathematical model being used and needs to be studied more to see if it is because of the reference parameters selected, a potential sign error in the mathematics, or a beneficial operating zone for rovers.

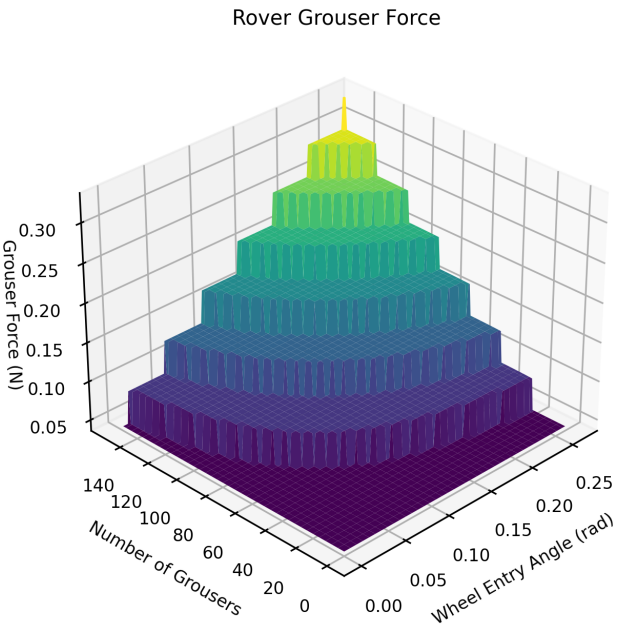

Fig. 5. Variation of the grouser force as a function of both the number of grousers ng and wheel entry angle θ_{en}. As modeled one would have to double the number of grousers on a wheel or double the entry angle before the estimated force changes. This highlights a limitation in the fundamental equations to handle changes in the number of grousers and leads to a more in-depth study into grouser forces to be undertaken.

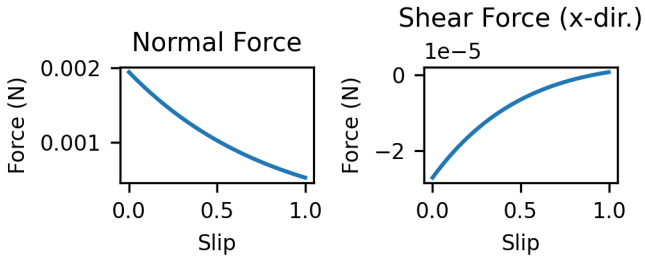

Fig. 6. The two plots shown here are the effect of slip on the normal force and the longitudinal shear force (shear force in the x direction). As slip increases the normal force decreases and the shear force approaches 0, however, the shear force is negative and is opposing the motion in this case, and thus increasing slip will initially benefit the rover's forward motion.

V. CONCLUSIONS

The parameter sensitivity of small-body rover dynamics conducted in this study shows that the most influential parameter in a rover's forward movement is the width of the wheels. This study was done for a specific set of reference parameters. A change in these parameters would thus result in the reported results being changed. The contribution of the paper is the numerical differential method used to calculate the partial derivatives as applied to small-body rovers; thus, the methodology of this study can be applied to any wheeled rover of interest. Additional work is needed to explore the relations of how varying multiple parameters at a time will

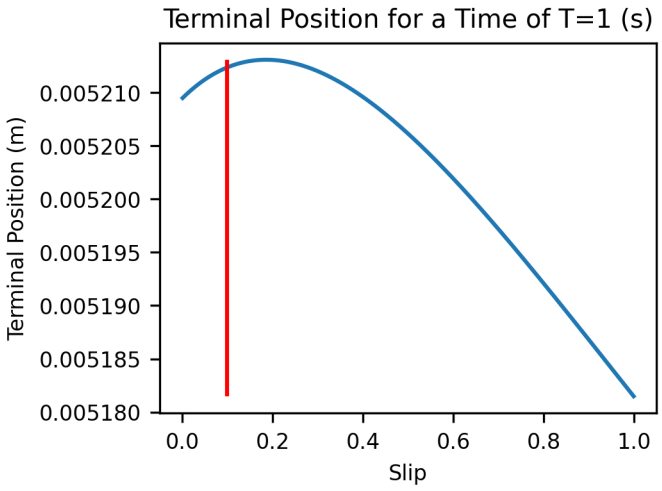

Fig. 7. This figure shows how the propagated position of a rover is affected by changes in the slip value. The vertical line is the reference value of the slip selected in this trial.

affect the motion of the rover. This analysis was conducted only considering the forward motion of the rover, but an extended 12 state (3 degrees of freedom position, linear velocity, orientation, and angular velocity) is currently being conducted by the authors. This paper thus serves as a starting point for the conversation of small body rover dynamic parameter sensitivity analysis.

REFERENCES

[1] [1] R. Chen, "Viper mission overview," NASA, https://www.nasa.gov/viper/overview (accessed Mar. 17, 2023).

[2] [1] E. Vitug, "Cooperative Autonomous Distributed Robotic Exploration (cadre)," NASA, https://www.nasa.gov/directorates/spacetech/game_changing_development/projects/CADRE (accessed Nov. 15, 2022).

[3] G. Ishigami, A. Miwa, K. Nagatani, and K. Yoshida, "Terramechanics-based model for steering maneuver of planetary exploration rovers on loose soil," Journal of Field Robotics, vol. 24, no. 3, pp. 233–250, Mar. 2007. doi:10.1002/rob.20187

[4] G. Ishigami, K. Nagatani and K. Yoshida, "Path Planning for Planetary Exploration Rovers and Its Evaluation based on Wheel Slip Dynamics," Proceedings 2007 IEEE International Conference on Robotics and Automation, Rome, Italy, 2007, pp. 2361-2366, doi: 10.1109/ROBOT.2007.363672.

[5] Zhou, F., Arvidson, R. E., Bennett, K., Trease, B., Lindemann, R., Bellutta, P., et al. (2013). Simulations of mars rover traverses 30, 10127–10134

[6] Wong, J.-Y. and Reece, A. R. (1967a). Prediction of rigid wheel performance based on the analysis of soil-wheel stresses part i. performance of driven rigid wheels. Journal of Terramchanics 4, 81–98

[7] Wong, J.-Y. and Reece, A. R. (1967b). Prediction of rigid wheel performance based on the analysis of soil-wheel stresses part ii. performance of towed rigid wheels. Journal of Terramchanics 4, 7–25

[8] Janosi, Z. and Hanamoto, B. (1961). Analytical determination of drawbar pull as a function of slip for tracked vehicles in deformable soils.

[9] J. Y. Wong, Theory of Ground Vehicles. New York: John Wiley, 2001.